Unprecedented Al supersaturation in single-phase rock salt structure VAlN films by Al+ subplantation

Grzegorz Greczynski, S. Mraz, M. Hans, D. Primetzhofer, Jun Lu, Lars Hultman and J. M. Schneider

Greczynski, G., Mraz, S., Hans, M., Primetzhofer, D., Lu, J., Hultman, L., Schneider, J. M., (2017), Unprecedented Al supersaturation in single-phase rock salt structure VAlN films by Al+ subplantation, *Journal of Applied Physics*, 121(17) . https://dx.doi.org/10.1063/1.4977813

Original publication available at:
https://dx.doi.org/10.1063/1.4977813

Unprecedented Al supersaturation in single-phase rock salt structure VAlN films by Al^+ subplantation

G. Greczynski,[1,2,*] S. Mráz,[2] M. Hans,[2] D. Primetzhofer,[3] J. Lu,[1] L. Hultman,[1] J.M. Schneider[2]

[1]*Thin Film Physics Division, Department of Physics (IFM), Linköping University, SE-581 83 Linköping, Sweden*
[2]*Materials Chemistry, RWTH Aachen University, Kopernikusstr. 10, D-52074 Aachen, Germany*
[3] *Department of Physics and Astronomy, The Ångström Laboratory, Uppsala University, P.O. Box 516, SE-75120 Uppsala, Sweden*

Abstract

Modern applications of refractory ceramic thin films, predominantly as wear-protective coatings on cutting tools and on components utilized in automotive engines, require a combination of excellent mechanical properties, thermal stability and oxidation resistance. Conventional design approaches for transition metal nitride coatings with improved thermal and chemical stability are based on alloying with Al. It is well known that the solubility of Al in NaCl-structure transition metal nitrides is limited. Hence, the great challenge is to increase Al concentration substantially while avoiding precipitation of thermodynamically-favored wurtzite-AlN phase which is detrimental to mechanical properties. Here, we use VAlN as a model system to illustrate a new concept for the synthesis of a metastable single-phase NaCl-structure thin films with Al content far beyond solubility limits obtained with conventional plasma processes. This supersaturation is achieved by separating the film-forming species in time and energy domains through synchronization of the 70-μs-long pulsed substrate bias with intense periodic fluxes of energetic Al^+ metal ions during reactive hybrid high power impulse magnetron sputtering of Al target and direct current magnetron sputtering of V target in Ar/N_2 gas mixture. Hereby, Al is subplanted

into the cubic VN grains formed by the continuous flux of low-energy V neutrals. We show that Al subplantation enables an unprecedented 42% increase in metastable Al solubility limit in $V_{1-x}Al_xN$, from $x = 0.52$ obtained with conventional method to 0.75. The elastic modulus is 325±5 GPa, in the excellent agreement with density functional theory calculations, and approximately 50% higher than for corresponding films grown by dc magnetron sputtering. The extension of the presented strategy to other Al-ion-assisted vapor deposition methods or materials systems is straightforward, which opens up the way for producing supersaturated single-phase functional ceramic alloy thin films combining excellent mechanical properties with high oxidation resistance.

1. Introduction

Transition metal (TM)-nitride-based thin layers for wear protective applications are often alloyed with Al to increase thermal stability and high-temperature oxidation resistance.[1,2] The challenge is then to maintain single phase NaCl-cubic (*c*) structure, avoiding precipitation of thermodynamically preferred softer wurtzite AlN phase (*w*-AlN) that is detrimental for coating properties.[3,4,5] Such metastable *c*-(TM)AlN compounds[6] can be obtained by physical vapor deposition due to kinetically-limited low-temperature growth and dynamic low-energy ion-irradiation-induced mixing in the near-surface region.[7] In conventional dc magnetron sputter (DCMS) deposition, reported kinetic AlN solubility limits in *c*-$(TM)_{1-x}Al_xN$ systems for growth temperatures T_s ~ 500 °C range from x = 0.3 for $Zr_{1-x}Al_xN$,[8] to 0.5 for $Ti_{1-x}Al_xN$,[9] and 0.67 for $Cr_{1-x}Al_xN$ compounds,[10] with some uncertainty related to the sensitivity of the analysis method used to detect precipitation of the *w*-AlN phase.[11,12] Supersaturated single-phase alloys with higher Al content are typically obtained by cathodic arc deposition, with x = 0.50 for ZrAlN,[13] 0.66 for TiAlN,[14,15,16] and 0.70 for CrAlN. The VAlN system is relatively less explored, with only few publications,[17,18,19] yet potentially useful predominantly due to the combination of high hardness and low friction coefficient, which makes it a promising candidate for applications as a wear-resistant coating in, for example, deep drawing of high-strength steels.[20]

It was recently shown that high-power impulse magnetron sputtering (HIPIMS)[21,22,23] provides an alternative route for ion-assisted TM nitride film growth via the use of a low duty cycle substrate bias synchronized to the metal-ion-rich portion of the plasma pulse.[24,25] Single-phase *c*-$Ti_{1-x}Al_xN$ films with x up to 0.65, combining high hardness (~30 GPa), high elastic modulus (~380 GPa), and low stress (0.2–0.8 GPa), were obtained with hybrid Al-HIPIMS/Ti-DCMS processing employing pulsed Al^+ ion irradiation and a synchronous negative substrate bias

V_s = -60 V, thus suppressing gas ion irradiation inherent to DCMS.[26,27,28] In a similar way, by exchanging Al for Si, metastable *c*-$Ti_{1-x}Si_xN$ solid solutions were demonstrated up to $x \leq 0.24$, *i.e.*, significantly higher Si concentrations than ever obtained by conventional magnetron sputtering methods.[29] These results reveal the essential role of metal-ion irradiation for the control of nanostructure formation and mechanical property evolution of metastable TM nitride based thin films.

Here, we present a novel approach to obtain supersaturated (TM)N thin film alloys with extremely high Al content. Using $V_{1-x}Al_xN$ as a model materials system and employing high-intensity temporal fluxes of Al^+ metal ions from pulsed HIPIMS source superimposed onto continuous flux of V neutrals from DCMS-operated target (hybrid Al-HIPIMS/V-DCMS co-sputtering), we are able to increase Al solubility limit to x_{max} = 0.75 from 0.52 obtained with conventional DCMS. The basic concept relies on implanting Al into already formed NaCl-structure grains, rather than allowing for gas ion-assisted competitive growth as is the case during DCMS. This is realized by separating the film-forming metallic species in time and energy domains.[24,30] 70-μs-long bias pulses with an amplitude of -300 V are applied synchronously with the Al^+-rich portion of HIPIMS discharge, to increase implantation depth of ionized Al. At all other times the substrate is floating at ca. -15 V, which suppresses intermixing due to gas ion bombardment and leads to *c*-VN-rich surface even for the case where time-averaged Al flux significantly exceeds that of V. Thus, single-phase *c*-VN crystallites dominate the surface and provide a template for subplanted Al^+ metal ions to crystallize in the metastable cubic structure rather than to nucleate second phase *w*-AlN. Resulting layers possess dense nanostructure and exhibit excellent mechanical properties even with *x* as high as 0.84.

2. Experimental Details

$V_{1-x}Al_xN$ films are grown on Si(001) substrates in an industrial CemeCon AG CC800/9 magnetron sputtering system,[31] equipped with two Advanced Energy Pinnacle Plus power supplies for DCMS operation. In addition, two external Melec SIPP2000USB-10-500-S pulsers with 10 kW ADL GX 100/1000 DC power supplies are used for HIPIMS and pulsed substrate bias. V and Al targets are assembled from two triangular pieces with purity >99.5 % that form rectangular plates with dimensions 8.8×50 cm². The stationary configuration is used. Substrates are mounted symmetrically with respect to the targets on the 120×310 mm^2 metal plate arranged in a co-sputtering geometry such that the angle between the substrate normal and the target normal is ~28°, and the target-to-substrate distance is 18 cm. The system base pressure is lower than 0.75 mPa (5.63×10^{-6} Torr), following the 1 h 40±5 min–long heating step, and the total pressure during deposition is 0.42 Pa (3 mTorr) with a nitrogen fraction in the sputtering gas, $N_2/(N_2+Ar)$, varied from 0.29 to 0.32. Substrate temperature T_s during deposition is ~500 °C.

Two series of $V_{1-x}Al_xN$ films with varying Al/(Al+V) ratio x are grown. First, a combinatorial approach is used with two identical Al/V targets operating in DCMS mode at 3 kW to deposit $V_{1-x}Al_xN$ films with x from 0.32 to 0.71, with a continuous DC bias V_s = -100 V. This particular choice of the substrate bias voltage is based on earlier reports where the growth of ternary VAlN films was demonstrated.[17,18] The second series is obtained using a hybrid process in which the Al target operates in HIPIMS mode, while the V target runs as a conventional magnetron (Al-HIPIMS/V-DCMS). The average HIPIMS power is set at 2.5 kW (pulsing frequency f = 500 Hz, pulse time τ_{HIP} = 50 μs), while the power to the DC magnetron is varied from 0.64 to 0.40 kW resulting in $V_{1-x}Al_xN$ compositions ranging from x = 0.68 to 0.84. Figure 1(a) shows typical target voltage *V(t)* and target current *I(t)* waveforms recorded during 50-μs long HIPIMS pulses. The

overall shape of *V(t)* and *I(t)* functions is essentially the same for all HIPIMS depositions and is characterized by a constant pulse voltage of 450 V and pulse current increasing linearly with time to reach ~470 A at the end of the pulse. A pulsed substrate bias (cf. Fig. 1(b)) is applied synchronously to the Al-HIPIMS pulses with the pulse length (70 μs for the x = 0.70 sample)[32] and offset (30 μs) synchronized to act predominantly on the metal-rich portion of the ion flux arriving at the substrate, as previously determined by time-resolved ion mass spectrometry measurements.[24] The amplitude is high V_s = -300 V in order to achieve significant metal ion penetration depths, while between HIPIMS pulses, the substrate is at floating potential, $V_f \simeq$ -15 V. Film thicknesses obtained from cross-sectional scanning electron microscopy (XSEM) analyses performed in a LEO 1550 instrument are in the range 1300-3300 nm (increasing with the Al content) for the 60-minutes long Al/V-DCMS depositions. In the case of Al-HIPIMS/V-DCMS series all layers are grown for 105 min., which results in 1000-1300 nm thick films.

θ-2θ x-ray diffraction (XRD) scans and $\sin^2\psi$ measurements for residual stress determinations,[33] are carried out using a Philips X'Pert MRD instrument operated with point-focus Cu Kα radiation. $V_{1-x}Al_xN$ relaxed lattice parameters a_o are determined from θ-2θ scans acquired at the strain-free tilt angle ψ^* defined as $\psi^* = arcsin\left[(2\nu/(1+\nu))^{1/2}\right]$,[33] in which ν is the Poisson ratio. As no $\nu(x)$ values are reported for $V_{1-x}Al_xN$ with $0 < x < 1$ we use linear extrapolation between 0.27 for VN (x = 0) and 0.24 for c-AlN (x = 1),[34] corresponding to ψ^* varying from ~41 to ~38°. The differential thermal contraction stress correction, which arises during cooling of the samples from T_s to RT, is calculated using the average thermal expansion coefficient of Si(001) α = 2.9×10^{-6} K^{-1}.[35] Since α for $V_{1-x}Al_xN$ films is unknown, we use a linear extrapolation between α_{VN} = 9.35×10^{-6} K^{-1} and α_{AlN} = 8.00×10^{-6} K^{-1} from Ref. 36.

The chemical composition of the as grown $V_{1-x}Al_xN$ films is determined by energy-dispersive *x*-ray spectroscopy (EDX) performed with EDAX instrument attached to JEOL scanning electron microscope JSM-6480, applying ZAF corrections. The stoichiometry of the most relevant VAlN film is also thoroughly characterized with time-of-flight energy elastic recoil detection analysis (ToF-E ERDA) employing a 5MV NEC instrument at the tandem accelerator laboratory (Uppsala University). For ToF-E ERDA a 36 MeV $^{127}I^{8+}$ probe beam is incident at 67.5° with respect to the sample surface normal, while recoils are detected at 45°. Apart from counting statistics, systematic uncertainties from two sources affect the evaluation: first, the uncertainty in the inelastic energy loss of the recoiling atom species enters concentrations and can in general lead to systematic uncertainties on a level of up to 10% with highest effects expected for heaviest recoiling particles. Second, the detection efficiency of the ToF-E telescope for light particles is found significantly below unity, which, however, for the present species of interest is expected of minor influence on the level of at most 2-3%. To minimize both sources of uncertainty, a comparison of ERDA-results with results obtained with Rutherford backscattering spectrometry (RBS) is made for an appropriate reference sample to reduce uncertainties to the one resulting from cumulative counting statistics of both experiments. This analysis confirms the accuracy of the determined concentrations for nitrogen within about 1-2%. The inter-comparison with RBS also indicates, that the deduced V concentrations from ERDA are possibly slightly overestimated (by up to 10%) on the expense of Al, indicating possibly even higher Al:V ratio.

3D atom probe tomography (APT) is used to investigate the lateral distribution of V, Al, and N in a CAMECA LEAP 4000X HR. Laser-assisted pulsing with 30 pJ energy and 250 kHz is carried out for field evaporation at 60 K specimen temperature and > 50 million ions are collected at a detection rate of 0.5%. Specimen preparation is done by a standard lift-out procedure[37] and

annular milling in a FEI HELIOS Nanolab 660 dual-beam focused ion beam microscope using Ga ions at 30 kV acceleration voltage to obtain a needle-like tip. Nanoindentation hardness *H* and elastic modulus *E* of $V_{1-x}Al_xN$ alloy films are obtained for each sample with a Berkovich diamond tip using a minimum of 20 indents, results are analyzed using the method of Oliver and Pharr.[38] Samples for cross-sectional TEM (XTEM) analyses are prepared by mechanical polishing, followed by Ar^+ ion milling at 5 kV with an 8° incidence angle and sample rotation. During the final thinning stages, the ion energy and incidence angle are reduced to 2.5 kV and 5°. Film microstructure is analyzed in an FEI Tecnai G2 TF 20 UT transmission electron microscope operated at 200 kV.

3. Computational Details

Experimentally determined lattice parameter and elastic modulus values are compared to density functional theory[39] calculations performed for $V_{0.28}Al_{0.72}N$ (space group $Fm\bar{3}m$) with the Vienna *ab initio* simulation package using projector augmented wave potentials. A 2×2×2 supercell with 64 atoms is chosen and 9 V as well as 23 Al atoms are distributed randomly on the metal sublattice, while the non-metal sublattice is occupied with 32 N atoms. The exchange energy is treated with the generalized gradient approximation,[40] while the tetrahedron method with Blöchl corrections is used for total energies.[41] An energy cut-off of 500 eV is employed, the convergence criterion for relaxation is 10^{-4} eV and Brillouin zone integration is carried out with a 6×6×6 Monkhorst-Pack k-point mesh.[42] Equilibrium volume and bulk modulus are obtained by energy minimization with respect to the volume using the Birch-Murnaghan equation of states.[43] The isotropic approximation $E = 3B(1-2\nu)$ serves for transformation of bulk modulus to elastic modulus assuming Poisson's ratio of $\nu = 0.29$.[44]

4. Results

Figure 2 shows two sets of θ-2θ x-ray diffraction scans obtained as a function of the sample tilt angle ψ (defined as the angle between surface normal and the diffraction plane containing the incoming and diffracted *x*-ray beams) varied from 0 to 71.57° for $V_{1-x}Al_xN$ alloy films with essentially identical Al content, $x \sim 0.70$, grown by (a) conventional DCMS, and (b) Al-HIPIMS/V-DCMS. Clearly, DCMS $V_{0.29}Al_{0.71}N$ film shows only wurtzite phase reflections $10\bar{1}0$, 0002, $10\bar{1}1$, and $10\bar{1}2$, shifted towards lower diffraction angles with respect to *w*-AlN powder diffraction patters,[45] indicating that films are exclusively composed of wurtzite phase expanded due to the incorporation of larger V atoms. Relaxed lattice parameters extracted from XRD peak positions are $a = 3.156$ Å and $c = 5.040$ Å, to be compared to 3.111 and 4.979 Å for bulk *w*-AlN.[45]

In contrast, $V_{0.30}Al_{0.70}N$ layers grown by Al-HIPIMS/V-DCMS exhibit only 111 and 002 NaCl structure diffraction peaks, shifted toward higher diffraction angles with respect to the reference *c*-VN powder patterns (e.g. $2\theta_{002} = 44.02°$ *vs.* 43.70° for powder sample)[46] due to incorporation of smaller Al atoms into the cubic lattice. The lattice shrinkage is, however, much smaller than in the case of well-studied TiAlN system,[26] due to the fact that the lattice mismatch between VN and *c*-AlN is only 0.5% *vs.* 2.9 % in the case of TiN.[47] The relaxed lattice parameter a_o extracted from the 002 peak position is 4.110 Å, which is in excellent agreement with 4.098 Å obtained by density functional theory calculations for *c*-$V_{0.28}Al_{0.72}N$ (deviation < 1%). Hence, we infer the formation of a metastable *c*-VAlN solid solution. The residual stress obtained from $\sin^2\psi$ analysis for the $V_{0.30}Al_{0.70}N$ film is -3.8 GPa.

The solid solution formation is further supported by the three-dimensional distribution of constitutional elements on the nm scale obtained by atom probe tomography (APT). A needle-like tip was prepared from the $V_{0.30}Al_{0.70}N$ Al-HIPIMS/V-DCMS film and a reconstruction is

presented for the atomic positions of V, Al and N in Figures 3(a)-3(c), characterized by a homogeneous concentration profile in growth direction as shown in Figure 3(d). The uniform distribution of all constituent atoms is confirmed by very good agreement of the measured distribution data with the calculated random (binomial) distribution in Figure 3(e).

The relative volume fractions χ of the second phase *w*-AlN precipitates, estimated from the 002 NaCl-structure and $10\bar{1}0$ wurtzite peak intensities integrated over all ψ angles and normalized to random powder diffraction values, are plotted in Figure 4(a) as a function of Al concentration x for both $V_{1-x}Al_xN$ film sets. This is a more precise method for estimating the relative phase content than typically used θ-2θ scans, as crystallites with various orientations with respect to the film normal are probed. In each sample series, there is a critical Al concentration value x_{max}, obtained from the linear extrapolations of $\chi(x)$ data points towards the $\chi = 0$ axis, above which the second phase is detected. Such determined x_{max} values correspond to the kinetic solubility limit of AlN in the NaCl crystal lattice and clearly exhibits a very large dependence on the growth method. With conventional DCMS growth $x_{max} = 0.52$ and is in a very good agreement with the previously reported value of 0.54 obtained with a DCMS process employing substrate rotation and significantly shorter target-to-substrate distance.[19] However, an unprecedented x_{max} of 0.75 is achieved by hybrid Al-HIPIMS/V-DCMS method with synchronous high-amplitude substrate bias.

Solubility limits have a direct effect on mechanical properties of $V_{1-x}Al_xN$ films as shown in Figures 4(b)-4(d), where nanoindentation hardness $H(x)$, elastic modulus $E(x)$, and the $H^3/E^2(x)$ ratio, reflecting materials resistance against plastic deformation[48] and considered an important parameter describing mechanical properties of nanostructured thin films,[49] are plotted as a function of Al content for both methods. For DCMS films, a rapid decrease in H is observed, from 29.3±1.3

GPa with $x \lesssim 0.45$ to, 22.4±1.6 and 13.9±2.0 GPa with $x = 0.51$ and 0.55. In a similar way, E drops from 408±10 GPa at lower x values to 315, 247 and even 211 GPa with $x = 0.55$, 0.62 and 0.71, respectively. Furthermore, the elastic modulus of the $V_{0.5}Al_{0.5}N$ single phase film shows, with a 10% deviation to the calculated value, good agreement with the *ab initio* prediction.[50] The H^3/E^2 ratio drops from 0.14±0.01 at lower x values to 0.07 and 0.03 with $x = 0.51$ and 0.55, respectively. Hence, values of all three parameters describing mechanical properties of $V_{1-x}Al_xN$ films can be rationalized based on the precipitation of the softer *w*-AlN phase.

Dramatically different mechanical properties are obtained for Al-HIPIMS/V-DCMS films, where H is high, ~30 GPa, even for $x = 0.70$ after which a slight decay with increasing Al content is observed to 28.2±0.3 GPa obtained with x as high as 0.84. E = 325±5 GPa with x in the range from 0.68 to 0.74, which is ~50% higher than for corresponding DCMS films, and drops to 274±5 GPa for $x \geq 0.80$. In a similar manner, H^3/E^2 ratio varies in the range from 0.25 with $x = 0.74$ to 0.31 for $x = 0.84$, a factor of ×2 higher value than measured for VAlN layers with similar Al content grown by conventional dc magnetron sputtering. The calculated elastic modulus for $V_{0.28}Al_{0.72}N$ is 325 GPa, hence, in excellent agreement with the experimental findings.

Two films with Al concentrations close to the respective solubility limits, one from each series, are selected for detailed microscopy studies. Figure 5(a) is a fracture XSEM micrograph obtained from the $V_{0.45}Al_{0.55}N$ alloy film grown by DCMS. A pronounced columnar structure is observed with an average column width of 200±20 nm with inter-columnar and intra-columnar porosity, a reflection of insufficient adatom surface mobilities,[7] which give rise to kinetic surface roughening,[51,52,53] exacerbated by atomic shadowing.[54] This assessment is confirmed by bright-field XTEM images acquired with two different magnifications and shown in Fig. 5(b). Porous nanostructure of DCMS films at high Al content was previously observed for VAlN layers grown

by a combination of DC and MF magnetron sputtering.[18] Selected area electron diffraction (SAED) pattern (see inset in Fig. 5(b)) reveals both NaCl (111, 002, and 220) as well as wurtzite ($11\bar{2}0$ and $10\bar{1}0$) diffraction rings in agreement with XRD results shown in Fig. 4(a), that indicate a relative *w*-AlN volume content in the x = 0.55 DCMS sample on the order of ~18 %.

In contrast, the $V_{0.30}Al_{0.70}N$ film grown with Al-HIPIMS/V-DCMS and high-amplitude substrate bias synchronized with the metal-rich portion of HIPIMS pulse exhibits fully-dense nanostructure with no open boundaries, as revealed by XSEM image (Fig. 5(c)), and confirmed by the bright-field XTEM (Fig. 5(d)). The SAED pattern clearly shows 111, 002, and 220 NaCl structure diffraction rings with no sign of *w*-AlN, indicating single cubic phase film, in agreement with XRD results in Fig. 2(b).

The EDX-determined composition of the *c*-$V_{0.30}Al_{0.70}N$ film grown with Al-HIPIMS/V-DCMS is confirmed by ToF-ERDA and APT analyses. Both techniques yield x = 0.71±0.1, in excellent agreement to the EDX result, which proves extremely high Al content in the NaCl-structure. In addition, ToF-ERDA indicates low oxygen content of 0.2 at%.

5. Discussion

The presented results illustrate tremendous potential of our novel approach for tuning properties of metastable *c*-(TM)N-based compounds through control of phase content. In order to elaborate a basic concept behind an increased Al solubility in the NaCl structure, we schematically compare both growth scenarios in Figure 6. In the conventional DCMS processing (see Fig. 6(a)), in addition to constant fluxes of low-energy V and Al neutrals, the film growth surface is subject to continuous irradiation by ~~inert~~ gas ions (primarily Ar^+ and N_2^+). Neglecting the potential energy terms, the ion energy can be expressed as $E_i = E_i^o + ne(V_s - V_{pl})$, in which E_i^o denotes the

average energy of ions entering the anode sheath, n accounts for the charge state of the ion, and V_{pl} is the plasma potential.[55] Since E_i^o is typically a few eV, n = 1, and V_{pl} ~15 V, E_i is essentially set by the amplitude of negative substrate bias. As the latter energy (~100 eV) is larger than the lattice displacement threshold, such ion bombardment leads to numerous collision cascade events in the near-surface region. This approach has been used extensively in the past during refractory TM nitride growth by conventional DC magnetron sputtering to overcome the characteristically underdense microstructures with rough surfaces of layers deposited at low temperatures (T_s/T_m < 0.3, where T_s and T_m: growth and melting temperature in K).[7] The effective depth of collision cascade events can be estimated from Monte-Carlo based TRIM (Transport of Ions in Matter)[56] simulations of ion/surface interactions and corresponds to the average V, Al, and atomic N primary recoil projected ranges ξ_V, ξ_{Al}, and ξ_N, accounting for straggle. For 100 eV Ar^+ ions (majority gas species) incident on the $V_{0.5}Al_{0.5}N$ surface, $\xi_V = \xi_{Al} = \xi_N$ = 12 Å, while the Ar^+ penetration depth is 15 Å. Thus, the first 15 Å of the top surface is subject to continuous intermixing, while the structure at larger depths is essentially frozen, as illustrated in Fig. 6(a). In the first approximation, the surface composition of film-forming species is defined by V and Al fluxes (neglecting resputtering and evaporation) and the N_2 partial pressure, hence, on average, the concentration profile is constant and equal to that in the bulk. For cases where V flux prevails over Al flux, formation rate of *c*-VN dominates providing a template for minority Al neutrals that are incorporated into the cubic phase resulting in formation of metastable VAlN. With increasing Al flux relative to that of V, the driving force for the formation of thermodynamically stable *w*-AlN phase increases. Eventually, during conventional DCMS growth, precipitation of the wurtzite phase is observed for $V_{1-x}Al_xN$ films with $x > x_{max}$ = 0.52, as shown in Figures 2(a), 4(a), and 5(b).

Entirely different deposition conditions are offered by our new growth concept, which is based on a separation of film-forming species in time and energy domains, as illustrated in Fig. 6(b). Here, in addition to a continuous flux of V neutrals from target operating in DCMS mode, that arrive with a sputter energy of a few eV, high fluxes of Al^+ metal ions originating from HIPIMS target are also periodically present. Time-resolved ion mass spectrometry analyses performed at the substrate position during Al-HIPIMS in Ar/N_2 atmosphere[24] indicate that the composition of the ion flux incident at the growing film varies during the HIPIMS pulse. Ar^+ and N_2^+ gas-ion irradiation dominates during the early (0-40 μs) and the later (>100 μs) stages, whereas between 40-100 μs the ion flux consists primarily of metal-ions (together with a minority Ar^+, N^+, and N_2^+ component) due to gas rarefaction associated with the high peak powers. Our idea for increasing the metastable solubility limit for Al relies on generating mobility on the metal sublattice through Al^+ subplantation into *c*-VN by synchronization of high-amplitude (-300 V) low duty cycle (3.5%) bias pulses with the Al^+-rich portion of the HIPIMS plasma. This is in contrast to conventional DCMS growth scenario, where Al is mobilized as a recoil during collision cascades initiated by continuous gas ion bombardment. For the remaining 96.5% of the time (between HIPIMS pulses), the growing film surface is at floating potential, $V_f \simeq$ -15 V, irradiated by gas ions (Ar^+ and N_2^+) that arrive with the energies below the lattice displacement threshold (~ 20-50 eV depending upon the ion and film species involved). Hence, the gas ion-induced atomic mixing is intentionally avoided. As a consequence, V and nitrogen fluxes deposited during this period, dominate the surface composition, even for the case where time-averaged Al flux significantly exceeds that of V, promoting the growth of *c*-VN phase, which in turn serves as a template for the subsequent implantation of Al^+ and nitrogen ions in the sub-surface region during the HIPIMS period. This subplantation takes place in the surface-near volume extending down to

25 Å, which is the actual penetration depth of ~300 eV Al^+ ions estimated with TRIM. In this volume, diffusion occurs, as the ion energy is larger than the lattice displacement threshold. Al^+ is subplanted into predetermined *c*-VN, which together with N^+ (TRIM-simulated penetration depth of 30 Å), generates the mobility required to form supersaturated *c*-VAlN. The supersaturated solid solution does not appear to decompose into *w*-AlN and *c*-VN, due to larger activation energies for diffusion in the bulk as compared to the surface. In distinct contrast, during the DCMS experiments, both film-forming metallic species coexist at the surface, where adatom diffusion prevents the supersaturation and instead leads to precipitation of *w*-AlN for $x = 0.52$, i.e., as soon as Al concentration significantly exceeds that of V (cf. Fig. 3(a)). Furthermore, it is evident that although N^+/N_2^+ ions are present during DCMS and are subplanted due to the V_s of -100 V (TRIM-simulated effective penetration depth of 15 Å) no supersaturation of the films can be obtained, which emphasizes the role of Al^+ subplantation-induced mobility on the cation lattice present during Al-HIPIMS/V-DCMS processing.

Based on the presented experimental evidence and the results of TRIM simulations, we conclude that the growth of supersaturated NaCl structure TM-nitride based films to large extent depends on the ionization degree of metal flux, metal-ion charge state, as well as, the separation of film forming species in time and energy domains.

The ionization degree in the HIPIMS plasma is closely related to the plasma density in front of the sputtering target and, thus, can be steered by the peak target current density.[57,58] Since the metal ionization is rarely close to 100%,[23,59] a substantial non-ionized metal fraction is deposited on the film surface, where adatom mobility counteracts the formation of supersaturated phase. This is acceptable for our purpose, however, as long as *x* at the surface does not exceed the kinetic solubility limit which, for simultaneously arriving and collocated Al and V atoms in our

model materials system of VAlN, equals ~0.5 (cf. DCMS results). Assuming that the entire ionized fraction of the metal flux α gets subplanted leading to an increased Al solubility in the cubic phase, one can express the solubility limit x_{max} as 1/(2-α). Since, in the present case, the experimentally determined x_{max} = 0.75 (see Fig. 3(a)) one can estimate that the ionization of Al flux at the substrate is on the order of ~67%, which seems very reasonable given the applied process conditions (target peak current density of ~1 A/cm^2 and target to substrate distance of 18 cm).[60] Higher ionization degrees may favor even higher solubility limits, however, there are restrictions as to how much the target peak current density (which affects ionization) can be increased before severe arcing occurs. Possible solutions to circumvent this problem, may rely on the use of other sources of metal ions than HIPIMS, as the general idea for an increased Al solubility through Al-subplantation is not necessarily limited to this one particular technique.

Ions of a single charge state are preferred as a simultaneous presence of differently-charged metal species introduces a risk for severe ion damage and resputtering upon application of high bias voltage necessary to achieve subplantation. The average metal-ion charge state during HIPIMS is to a large extent determined by the second ionization potential of a metal IP_{Me}^2 with respect to the first ionization potential of the sputtering gas IP_g^1.[61] Metal-ion flux to the substrate is dominated by singly-charged ions if $IP_{Me}^2 > IP_g^1$, which is the case for Al target sputtered in Ar/N_2, for which IP_{Al}^2 = 18.83 eV (IP_{Ar}^1 = 15.76 eV, and $IP_{N_2}^1 = 15.55$ eV),[62] and gas ionization depletes the population of electrons with $E_e > IP_{Ar}^1$. For metals with IP_{Me}^2 lower than that of Al, one can decrease the doubly-ionized metal fraction by introducing noble gases with low IP_g^1 (e.g. Kr or Xe) so that $IP_{Me}^2 > IP_g^1$ is still satisfied.[61]

Finally, the substrate bias pulses applied synchronously with the HIPIMS pulse at the cathode have to be carefully designed to ensure sufficient separation of film-forming species in

time and energy domains. The former requires that both, the offset with respect to the cathode pulse as well as the pulse length are optimized to obtain maximum metal-ion/noble-gas-ion ratio in the flux incident at the growing film surface. This is to obtain significant metal subplantation while avoiding incorporation of noble gas atoms that occupy interstitial lattice sites which increases residual stresses,[7,63,64] causes gas bubble formation at higher operating temperatures,[65] and eventually leads to cohesive failure and film/substrate delamination. Ideally, the time-resolved ion mass spectrometry performed at the substrate position allows for precise measurement of the metal- and gas-ion flux time evolution during the HIPIMS pulse, which then can serve as an input for precise timing of V_s pulses.[27] Separation of film-forming species in the energy domain requires that the amplitude of the synchronized bias pulse is high enough so that metal ions accelerated in the electric field of the substrate are able to penetrate the growing film surface, going pass the high mobility surface layer, and become subplanted into the *c*-VN-rich grains generating the mobility required to form supersaturated VAlN phase. To serve this purpose the preferred implantation depths should be in the range 10-25 Å. Here, TRIM simulations of ion/solid interactions can be used to provide guidelines for particular choices of materials system.

6. Conclusions

We demonstrate a new processing strategy for growth of Al-supersaturated cubic-phase $V_{1-x}Al_xN$. Al subplantation enables an unprecedented 42% increase in metastable Al solubility limit, from $x = 0.52$ obtained with conventional magnetron sputtering techniques to $x_{max} = 0.75$. The novel process is based on separating the film forming metallic species in time and energy domains, which is realized by employing high-intensity temporal fluxes of Al^+ metal ions from pulsed HIPIMS source superimposed onto a continuous V neutral flux supplied from a DCMS-operated target (hybrid Al-HIPIMS/V-DCMS co-sputtering). For 96.5% of the deposition time,

the growing film surface is irradiated by gas ions arriving with the energies below the lattice displacement threshold, which suppresses the atomic mixing and leads to the formation of cubic VN, even for the case where time-averaged Al flux significantly exceeds that of V. Then, during the low-duty-cycle (3.5%) metal-rich HIPIMS phase, high-energy Al^+ ions are subplanted into *c*-VN grains, which together with a simultaneous supply of N^+ generates the required mobility on the cation lattice to form a supersaturated *c*-VAlN solid solution. Experimental evidence for this effect is given by X-ray diffraction and atom probe tomography that show no decomposition i.e. the formation of *w*-AlN. This is due to the larger activation energies for mass transport in the bulk volume as compared to the surface. In contrast, during conventional dc magnetron sputtering experiments both film-forming metallic species coexist at the surface where adatom diffusion and gas-ion-induced mixing prevent the formation of supersaturated *c*-VAlN and the precipitation of *w*-AlN is observed when the Al concentration exceeds that of V.

The present high Al-content *c*-VAlN films grown by the Al^+-subplantation technique exhibit fully-dense nanostructure and excellent mechanical properties with hardness in the range of 28-30 GPa for Al fractions on the cation lattice as high as 84%. The elastic modulus is with 325±5 GPa in the excellent agreement with density functional theory calculations, and approximately 50% higher than for films grown by DCMS. This substantial improvement with respect to the conventional techniques opens the way for synthesis of supersaturated single-phase alloy thin films combining excellent mechanical properties with high oxidation resistance. Extensions of the presented method to other materials systems are expected to be straightforward.

Acknowledgements

The authors most gratefully acknowledge the financial support of the German Research Foundation (DFG) within SFB-TR 87, the VINN Excellence Center *Functional Nanoscale*

Materials (FunMat) Grant 2005-02666, the Swedish Government Strategic Research Area in Materials Science on Functional Materials at Linköping University (Faculty Grant SFO-Mat-LiU 2009-00971), a research infrastructure fellowship of the Swedish Foundation for Strategic Research (SSF) under contract RIF14-0053, the Åforsk Foundation Grant 16-359, and the Knut and Alice Wallenberg Foundation Grant 2011.0143. Density functional theory calculations were performed with computing resources granted by JARA-HPC from RWTH Aachen University under project JARA0131.

Figure captions

Fig. 1. (a) target voltage and target current waveforms recorded during the50-μs-long Al-HIPIMS/V-DCMS discharge, along with (b) substrate voltage and substrate current.

Fig. 2. XRD θ-2θ scans as a function of the tilt angle ψ for (a) x = 0.71 DCMS, and (b) x = 0.70 Al-HIPIMS/V-DCMS $V_{1-x}Al_xN$ layers.

Fig. 3. Atomic positions of (a) V, (b) Al, and (c) N in the reconstruction of a $V_{0.30}Al_{0.70}N$ tip obtained by atom probe tomography, (d) concentration profile for a distance of 200 nm in growth direction, and (e) the frequency distribution analysis, comparing the measured and calculated random (binomial) distribution data.

Fig. 4. (a) $10\bar{1}0$ *w*-AlN and 002 *c*-VN peak area ratios integrated over all ψ angles and normalized to random powder XRD patterns plotted as a function of x for $V_{1-x}Al_xN$ films grown by conventional DCMS and hybrid Al-HIPIMS/V-DCMS method with high-amplitude substrate bias synchronized to the metal-rich portion of HIPIMS pulses, (b) nanoindentation hardness $H(x)$, (c) elastic modulus $E(x)$, and (d) $H^3/E^2(x)$ ratio obtained from both sets of $V_{1-x}Al_xN$ alloy films.

Fig. 5. (a) XSEM and (b) bright field XTEM images obtained from the $V_{0.45}Al_{0.55}N$ film grown with conventional DCMS. Higher magnification XTEM image and SAED pattern are shown as insets in (b). (c) XSEM and (d) bright-field XTEM images together with a corresponding SAED patterns for $V_{0.30}Al_{0.70}N$ films grown by hybrid Al-HIP/V-DC method with high-amplitude substrate bias synchronized to the metal-rich portion of HIPIMS pulses.

Fig. 6. Schematic representation of the growth process for high-Al content VAlN films (x = 0.60): (a) conventional dc magnetron sputtering and (b) hybrid Al-HIPIMS/V-DCMS processing with high-amplitude substrate bias synchronized to the Al-rich portion of HIPIMS pulses.

References:

[1] H. Schulz, K.H. Thiermann, *Solid State Communications* 23, 815 (1977)
[2] O. Knotek, M. Böhmer, T. Leyendecker, *J. Vac. Sci. Technol. A* 4 (1986) 2695
[3] A.E. Reiter, V.H. Derflinger, B. Hanselmann, T. Bachmann, and B. Sartory, *Surf. Coat. Technol.* 200 (2005) 2114
[4] A. Kimura, H. Hasegawa, K. Yamada, T. Suzuki, *Surf. Coat. Techn*ol. 120–121 (1999) 438
[5] A. Hörling, L. Hultman, M. Odén, J. Sjölén and L. Karlsson, *Surf. Coat. Technol*. 191 (2005) 384
[6] P.H. Mayrhofer, D. Music, J.M. Schneider, *Appl. Phys. Lett.* 100 (2006) 094906
[7] I. Petrov, P.B. Barna, L. Hultman, and J.E. Greene, J. Vac. Sci. Technol. A 21, S117 (2003)
[8] Y. Makino, M. Mori, S. Miyake, K. Saito, and K. Asami, *Surf. Coat. Technol.* 193 (2005) 219
[9] U. Wahlström, L. Hultman, J.-E. Sundgren, F. Adibi, I. Petrov and J. E. Greene, *Thin Solid Films* 235 (1993) 62
[10] A. Sugishima, H. Kajioka, Y. Makino, *Surf. Coat. Technol* 97 (1997) 590
[11] R. Rachbauer, S. Massl, E. Stergar, D. Holec, D. Kiener, J. Keckes, J. Patscheider, M. Stiefel, H. Leitner, and P. H. Mayrhofer, *J. Appl. Phys.* 110 (2011) 023515
[12] M. to Baben, M. Hans, D. Primetzhofer, S. Evertz, H. Ruess, and J. M. Schneider, *Mater. Res. Lett.* (2016) http://dx.doi.org/10.1080/21663831.2016.1233914
[13] H. Hasegawa, M. Kawate, T. Suzuki, *Surf. Coat. Technol* 200 (2005) 2409
[14] A. Hörling, L. Hultman, M. Odén, J. Sjölén, L. Karlsson *Thermal Stability of arc evaporated high aluminium-content* $Ti_{1-x}Al_xN$ *thin films* J. Vac. Sci. Technol. A 20 (2002) 1815
[15] J.M. Andersson, J. Vetter, J. Müller, J. Sjölén, *Surf. Coat. Technol*. 240 (2014) 211
[16] J. Vetter, *J. Adv. Mat.*, 31 (1999) 41
[17] S. Kolozsvári, P. Pesch, C. Ziebert, M. Stueber, S. Ulrich, *Plasma Process. Polym*. 6 (2009) S146
[18] P. Zhu, F. Ge, S. Li, Q. Xue, F. Huang, *Surf. Coat. Technol.* 232 (2013) 311
[19] F. Rovere, D. Music, S. Ershov, M. to Baben, H-G. Fuss, P. H Mayrhofer, and J. M. Schneider, *J. Phys. D: Appl. Phys*. 43 (2010) 035302
[20] M. Liewald, S. Wagner, D. Becker, C. Ziebert, P. Pesch, and S. Kolozsvári, *Int. J. Adv. Manuf. Technol.* 58 (2012) 495
[21] V. Kouznetsov, K. Macak, J. M. Schneider, U. Helmersson and I. Petrov, *Surf. Coat. Technol.* 122 (1999) 290
[22] U. Helmersson, M. Lattemann, J. Bohlmark, A.P. Ehiasarian, J.T. Gudmundsson, *Thin Solid Films* 513 (2006) 1
[23] K. Sarakinos, J. Alami, S. Konstantinidis, *Surf. Coat. Technol.* 204 (2010) 1661
[24] G. Greczynski, J. Lu, J. Jensen, I. Petrov, J.E. Greene, S. Bolz, W. Kölker, Ch. Schiffers, O. Lemmer and L. Hultman, *J. Vac. Sci. Technol. A* 30 (2012) 061504.
[25] G. Greczynski, J. Lu, J. Jensen, S. Bolz, W. Kölker, Ch. Schiffers, O. Lemmer, J.E. Greene, and L. Hultman, *Surf. Coat. Technol*. 257 (2014) 15.
[26] G. Greczynski, J. Lu, J. Jensen, I. Petrov, J.E. Greene, S. Bolz, W. Kölker, Ch. Schiffers, O. Lemmer and L. Hultman, *Thin Solid Films* 556 (2014) 87
[27] G. Greczynski, J. Lu, M. Johansson, J. Jensen, I. Petrov, J.E. Greene, and L. Hultman, *Surf. Coat. Technol*. 206 (2012) 4202.
[28] G. Greczynski, J. Lu, M. Johansson, J. Jensen, I. Petrov, J.E. Greene, and L. Hultman, *Vacuum* 86 (2012) 1036.
[29] G. Greczynski, J. Patscheider, J. Lu, B. Alling, A. Ektarawong, J. Jensen, I. Petrov, J. E. Greene, L. Hultman, *Surf. Coat. Technol.* 280 (2015) 174
[30] K. Macak, V. Kouznetsov, J. Schneider, U. Helmersson and I. Petrov, *J. Vac. Sci. Technol. A* 18 (2000) 1533
[31] http://www.cemecon.de/coating_technology/coating_units/hipims_sputter_coating_system/index_eng.html, accessed in February 2015
[32] For all other Al-HIPIMS/V-DCMS VAlN films the bias pulse length was 100 μs
[33] See, e.g., Chapter 6 in M. Birkholz *Thin Film Analysis by X-ray Scattering*, ISBN-10: 3-527-31052-5, Wiley-VCH, Weinheim 2006.
[34] B. D. Fulcher, X. Y. Cui, B. Delley, C. Stampfl, Phys. Rev. B 85 (2012) 184106
[35] H. Watanabe, N. Yamada, M. Okaji, Int. J. Thermophys. 25, 221 (2004).
[36] Hugh O. Pierson (1996). *Handbook of refractory carbides and nitrides: properties, characteristics, processing, and applications*. William Andrew. p. 193. ISBN 0-8155-1392-5.

[37] T. F. Kelly, D. J. Larson, Atom probe tomography 2012, *Annu. Rev. Mater. Res.* 42 (2012) 1-31
[38] W. C. Oliver and G. M. Pharr, *J. Mater. Res.* 7 (1992) 1564.
[39] P. Hohenberg, W. Kohn, *Phys. Rev.* 136 (1964) B864-B871
[40] J. P. Perdew, K. Burke, M. Enzerhof, *Phys. Rev. Lett.* 77 (1996) 3865-3868
[41] P. E. Blöchl, O. Jepsen, O. K. Andersen, *Phys. Rev. B* 49 (1994) 16223-16233
[42] H. J. Monkhorst, D. J. Pack, *Phys. Rev. B* 13 (1976) 5188-5192
[43] F. Birch, *J. Geophys. Res*. 83 (1978) 1257-1268
[44] A. Mei, R. B. Wilson, D. Li, D.G. Cahill, A. Rockett, J. Birch, L. Hultman, J. E. Greene, and I. Petrov, *J. Appl. Phys*. 115 (2014) 214908
[45] The JCPDS database (1998), data set number: 25-1133
[46] The JCPDS database (1998), data set number: 35-0768;
[47] The JCPDS database (1998), data set number: 38-1420; W. Wong-Ng, H. McMurdie, B. Paretzkin, C. Hubbard, A. Dragoo, Powder Diffraction 2, 2 (1987).
[48] T.Y. Tsui, G.M. Pharr, and W.C. Oliver, *Mater. Res. Soc. Symp. Proc.* 383 (1995) 447
[49] J. Musil *Surf. Coat. Technol*. 125 (2000) 322
[50] K.P. Shaha, H. Ruess, S. Rotert, M. to Baben, D. Music, and J. M. Schneider, *Appl. Phys. Lett*. 103 (2013) 221905
[51] N.-E. Lee, D.G. Cahill, J.E. Greene, *J. Appl. Phys.* 80, 2199 (1996).
[52] J. Krug, P. Politi, T. Michely, *Phys. Rev. B* 61, 14037 (2000).
[53] B.W. Karr, I. Petrov, D.G. Cahill, and J.E. Greene, Appl. Phys. Lett. 70**,** 1703 (1997).
[54] C. Roland and H. Guo, *Phys. Rev. Lett.* 66**,** 2104 (1991).
[55] A. Anders, *Appl. Phys. Lett*. 80 (2002) 1100
[56] J. F. Ziegler, J. P, Biersack, U. Littmark, "The Stopping and Range of Ions in Solids," vol. 1 of series "Stopping and Ranges of Ions in Matter," Pergamon Press, New York (1984).
[57] J. Böhlmark, J. Alami, C. Christou, A.P. Ehiasarian, U. Helmersson, *J. Vac. Sci. Technol. A* 23 (2005) 18
[58] G. Greczynski, J. Jensen, L. Hultman, *Thin Solid Films* 519 (2011) 6354–6361
[59] U. Helmersson, M. Lattemann, J. Bohlmark, A. P. Ehiasarian, and J. T. Gudmundsson, *Thin Solid Films* 513 (2006) 1
[60] G. Greczynski and L. Hultman, *Vacuum* 124 (2016) 1
[61] G. Greczynski, I. Petrov, J.E. Greene, and L. Hultman, *Vacuum* 116 (2015) 36
[62] David R. Lide (ed), *CRC Handbook of Chemistry and Physics, 84th Edition*. CRC Press. Boca Raton, Florida, 2003; Section 10, Atomic, Molecular, and Optical Physics; Ionization Potentials of Atoms and Atomic Ions.
[63] J.E. Greene, "Thin Film Nucleation, Growth, and Microstructural Evolution: an Atomic Scale View," in *Handbook of Deposition Technologies for Thin Films and Coatings*, Third Edition, ed. by P. Martin, William Andrew Publications (Elsevier), Burlington, MA (2010)
[64] J.M.E. Harper, J.J. Cuomo, R.J. Gambino, *Ion Bombardment Modification of Surfaces: Fundamentals and Applications*, Edited by O. Auciello and R. Kelly (Elsevier, Amsterdam, 1984).
[65] L. Hultman, J.-E. Sundgren, L.C. Markert, J.E. Greene *J. Vac Sci. Technol.* A 7 (1989) 1187

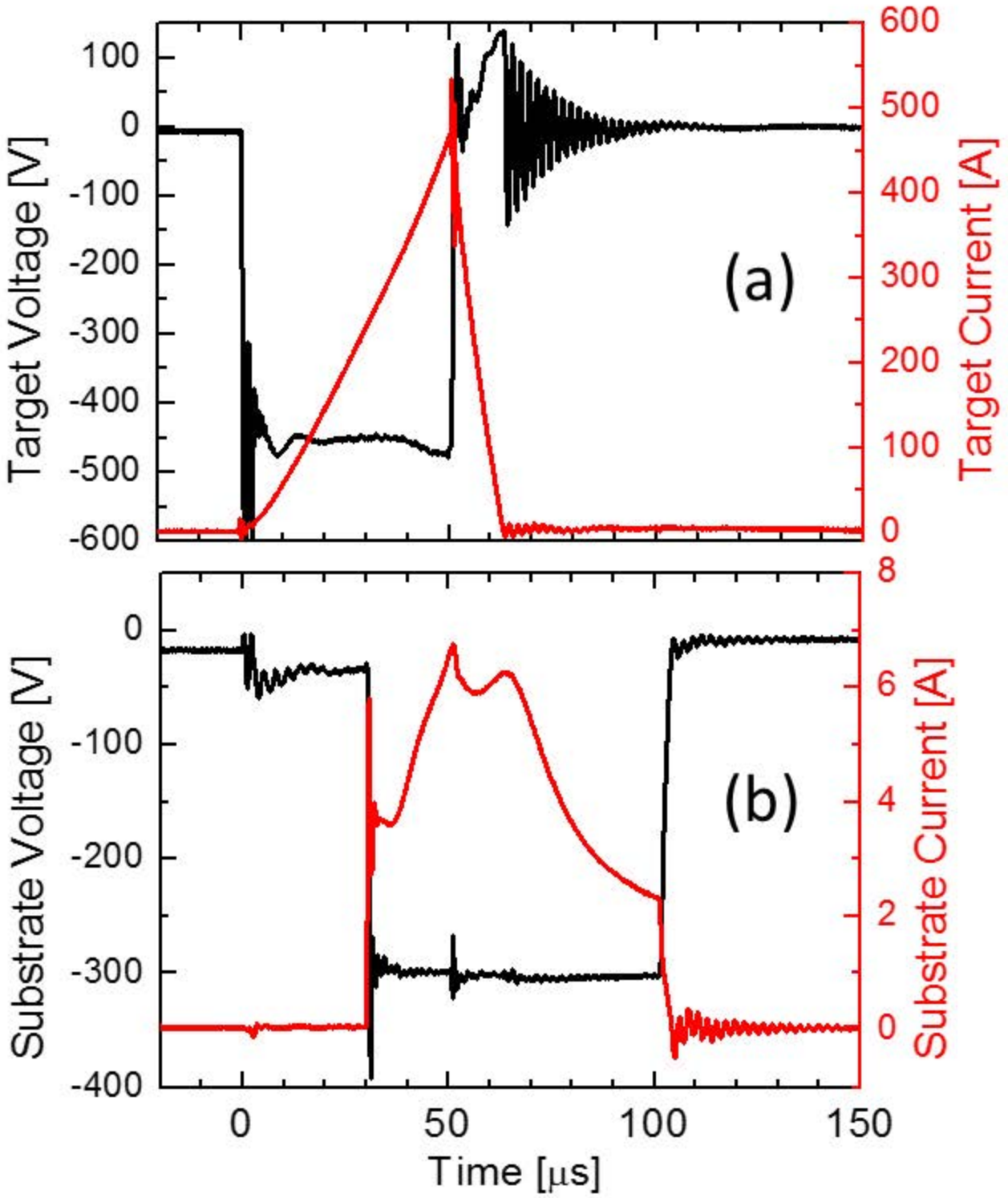
Target Voltage [V]
Target Current [A]
(a)
Substrate Voltage [V]
Substrate Current [A]
(b)
Time [μs]
100
0
-100
-200
-300
-400
-500
-600
600
500
400
300
200
100
0
8
6
4
2
0
-400
50
150

Fig. 1

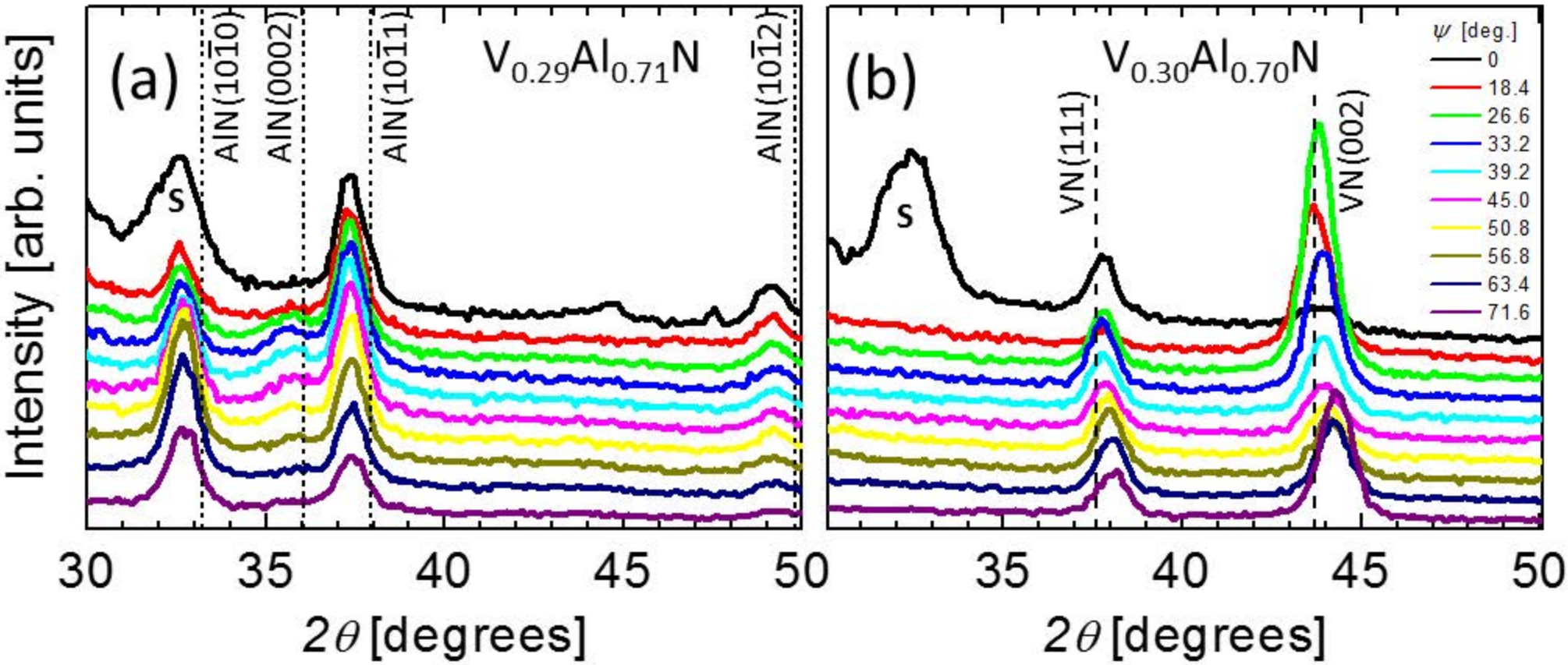
(a)
$V_{0.29}Al_{0.71}N$
AlN(10$\bar{1}$0)
AlN(0002)
AlN(10$\bar{1}$1)
AlN(10$\bar{1}$2)
s
(b)
$V_{0.30}Al_{0.70}N$
VN(111)
VN(002)
s
ψ [deg.]
0
18.4
26.6
33.2
39.2
45.0
50.8
56.8
63.4
71.6
Intensity [arb. units]
30
35
40
45
50
2θ [degrees]
35
40
45
50
2θ [degrees]

Fig. 2

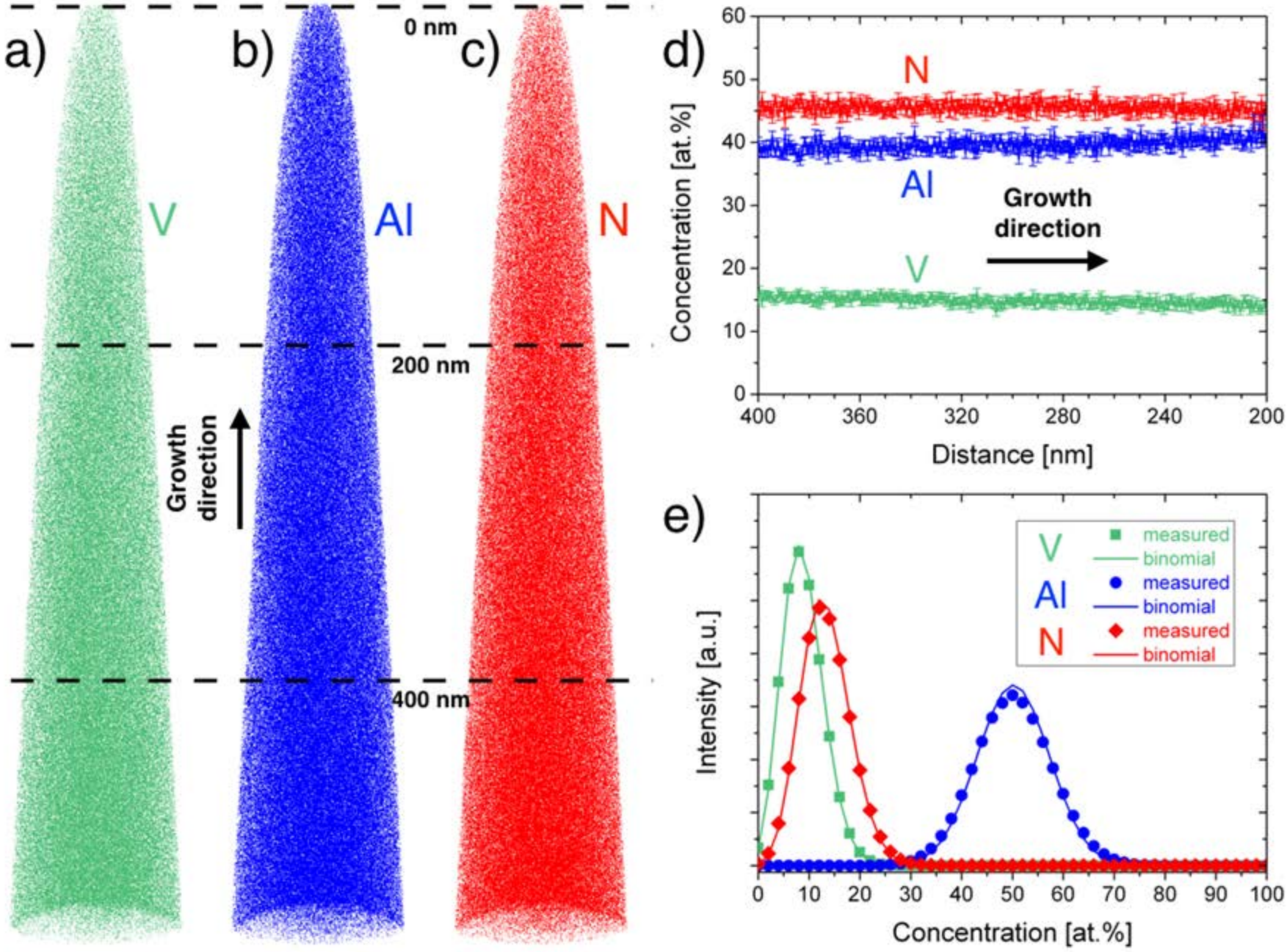
a)
b)
c)
0 nm
200 nm
400 nm
V
Al
N
Growth direction
d)
N
Al
V
Growth direction
Concentration [at.%]
Distance [nm]
e)
V
Al
N
measured
binomial
measured
binomial
measured
binomial
Intensity [a.u.]
Concentration [at.%]

Fig. 3

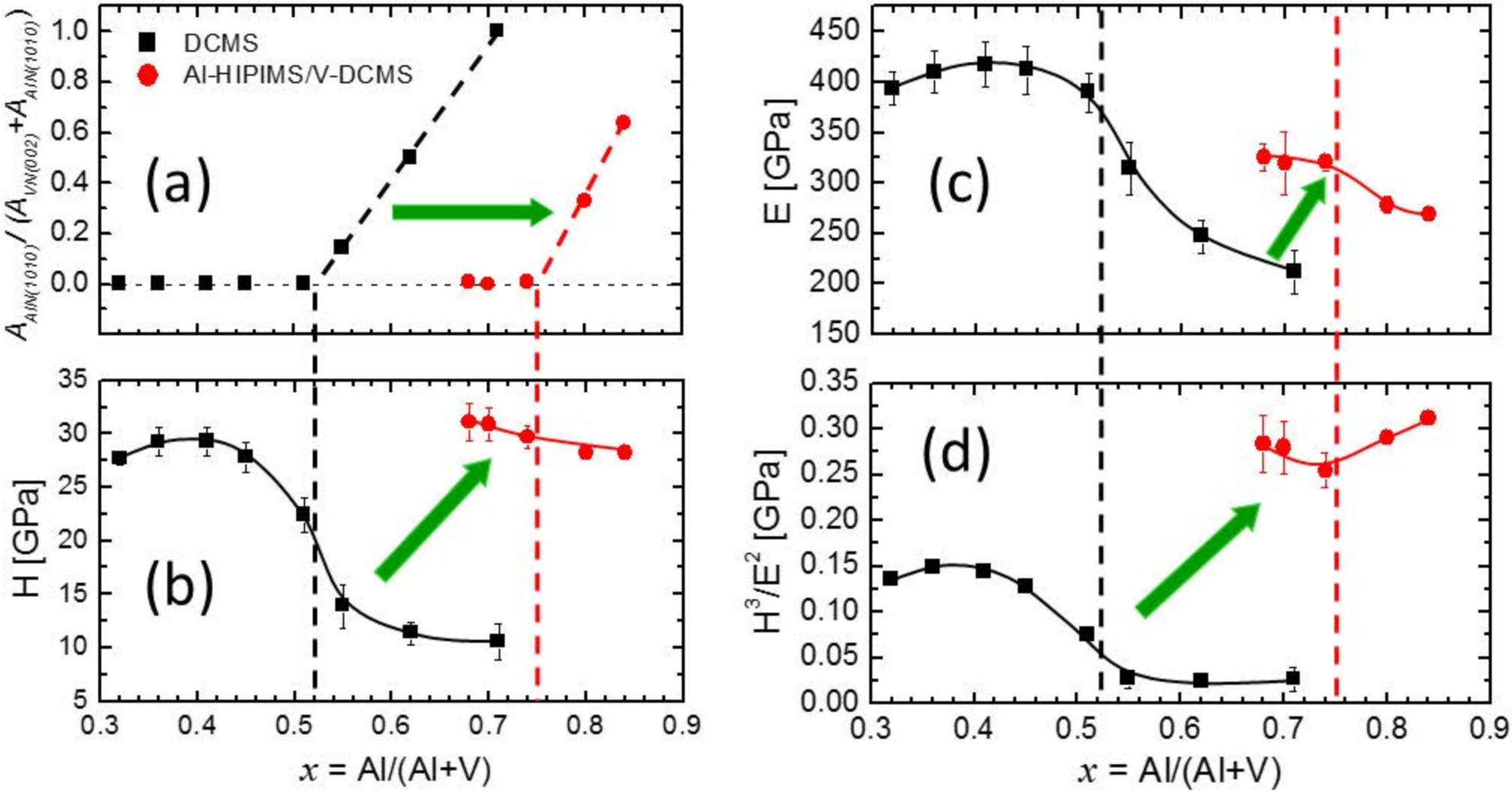
DCMS
Al-HIPIMS/V-DCMS
(a)
(b)
(c)
(d)
$A_{AlN(1010)} / (A_{VN(002)} + A_{AlN(1010)})$
H [GPa]
E [GPa]
H^3/E^2 [GPa]
x = Al/(Al+V)
x = Al/(Al+V)

Fig. 4

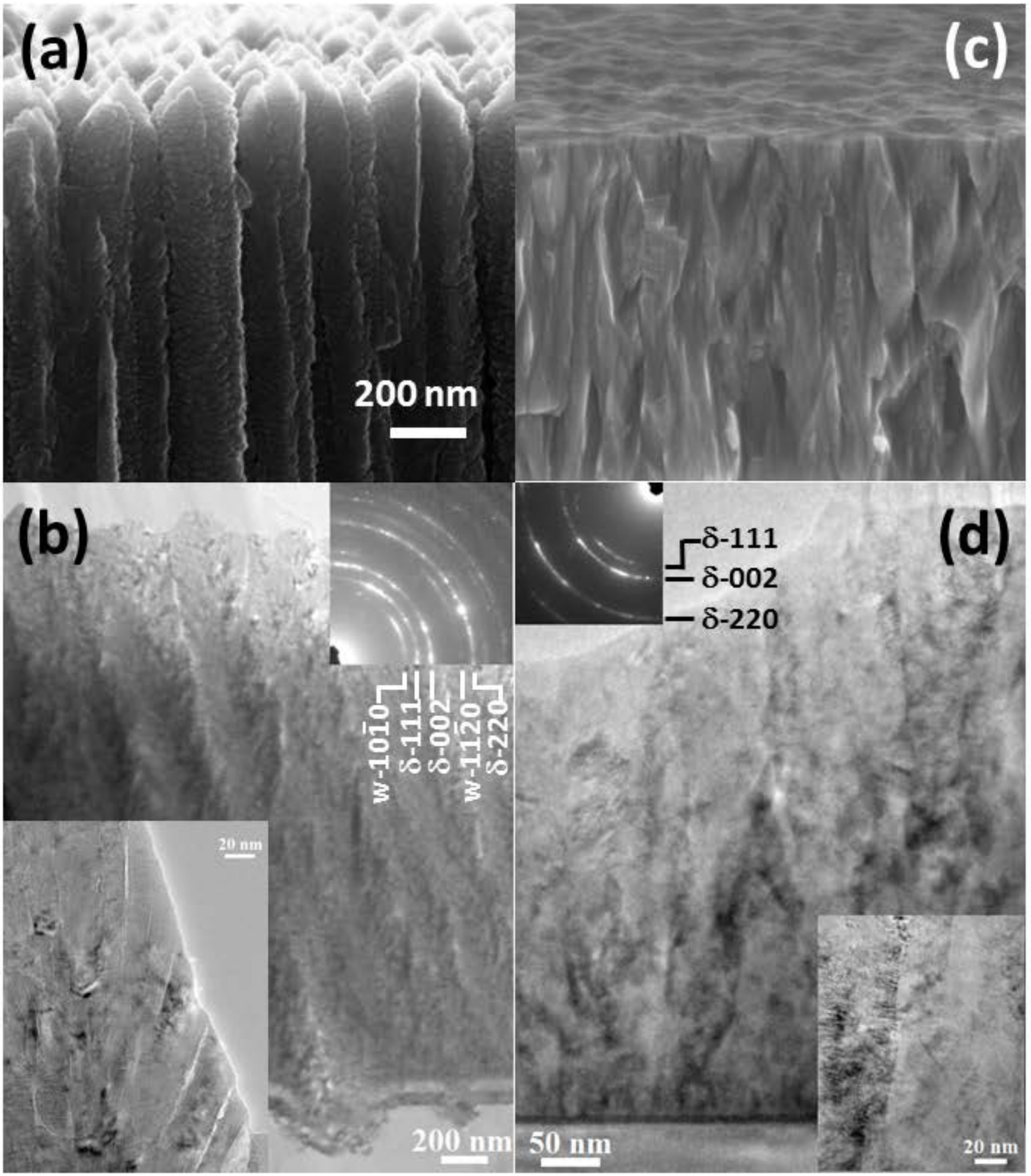
(a)
200 nm
(c)
(b)
w-10$\bar{1}$0
δ-111
δ-002
w-11$\bar{2}$0
δ-220
20 nm
200 nm
(d)
δ-111
δ-002
δ-220
50 nm
20 nm

Fig. 5

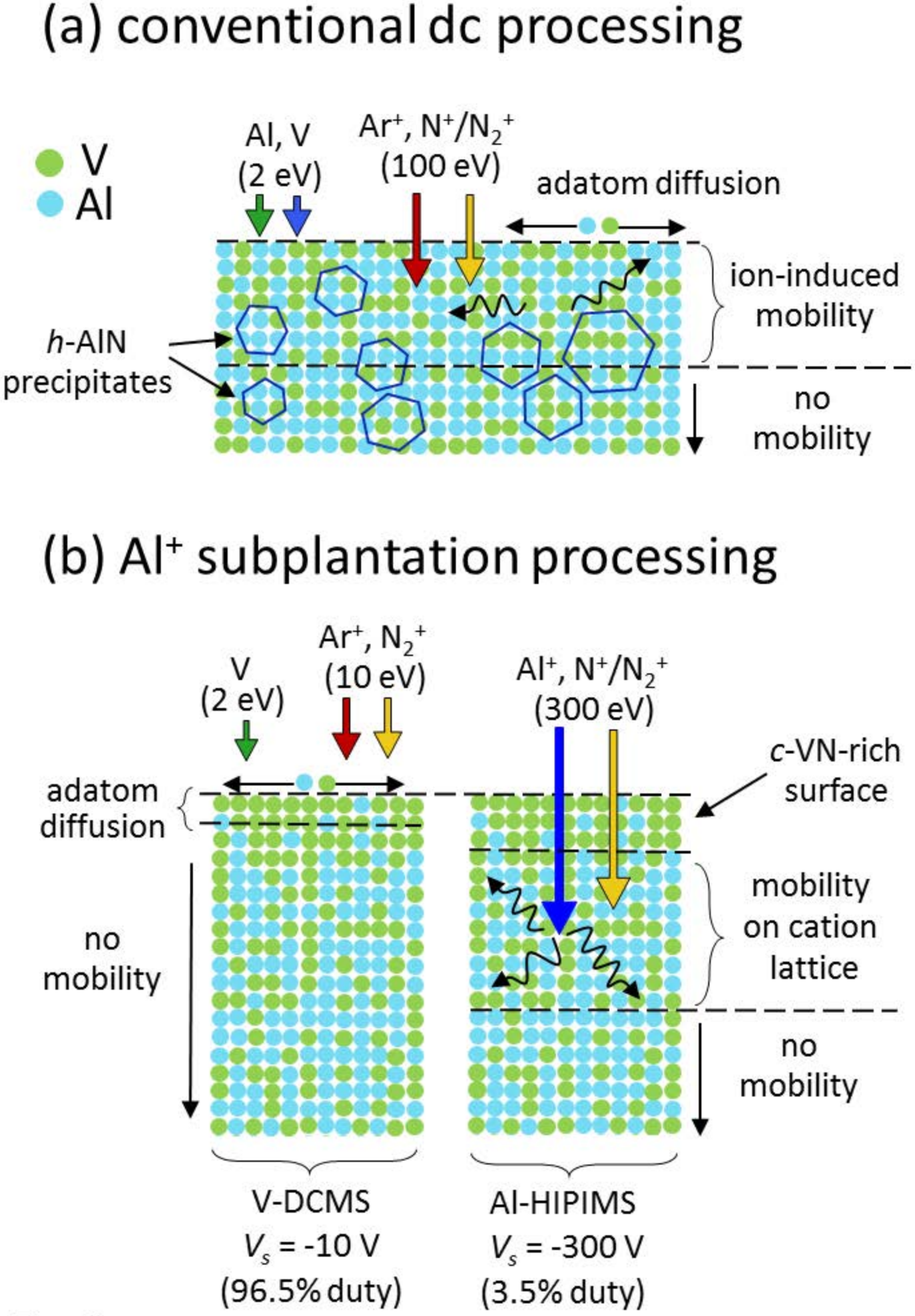
(a) conventional dc processing
V
Al
Al, V
(2 eV)
Ar+, N+/N2+
(100 eV)
adatom diffusion
ion-induced
mobility
h-AlN
precipitates
no
mobility
(b) Al+ subplantation processing
Ar+, N2+
(10 eV)
V
(2 eV)
Al+, N+/N2+
(300 eV)
c-VN-rich
surface
adatom
diffusion
mobility
on cation
lattice
no
mobility
no
mobility
V-DCMS
Vs = -10 V
(96.5% duty)
Al-HIPIMS
Vs = -300 V
(3.5% duty)

Fig. 6